Bull Volcanol (1986) 48: 245-264

Bulletin of
Volcanology

Explosive magma-water interactions: Thermodynamics, explosion mechanisms, and field studies

Kenneth H Wohletz

Earth and Space Science Division, Los Alamos National Laboratory, Los Alamos, NM 87545, USA

Abstract. Physical analysis of explosive, magma-water interaction is complicated by several important controls: (1) the initial geometry and location of the contact between magma and water; (2) the process by which thermal energy is transferred from the magma to the water; (3) the degree to and manner by which the magma and water become intermingled prior to eruption; (4) the thermodynamic equation of state for mixtures of magma fragments and water; (5) the dynamic metastability of superheated water; and (6) the propagation of shock waves through the system. All of these controls can be analyzed while addressing aspects of tephra emplacement from the eruptive column by fallout, surge, and flow processes. An ideal thermodynamic treatment, in which the magma and external water are allowed to come to thermal equilibrium before explosive expansion, shows that the maximum system pressure and entropy are determined by the mass ratio of water and magma interacting. Explosive (thermodynamic) efficiency, measured by the ratio of maximum work potential to thermal energy of the magma, depends upon heat transfer from the pyroclasts to the vapor during the expansion stage. The adiabatic case, in which steam immediately separates from the tephra during ejection, produces lower efficiencies than does the isothermal case, in which heat is continually transferred from tephra to steam as it expands. Mechanisms by which thermal equilibrium between water and magma can be obtained require intimate mixing of the two. Interface instabilities of the Landau and Taylor type have been documented by experiments to cause fine-scale mixing prior to vapor explosion. In these cases, water is heated rapidly to a metastable state of superheat where vapor explosion occurs by spontaneous nucleation when a temperature limit is exceeded. Mixing may also be promoted by shock wave propagation. If the shock is of sufficient strength to break the magma into small pieces, thermal equilibrium and vapor production in its wake may drive the shock as a thermal detonation. Because these mechanisms of magma fragmentation allow calculation of grain size, vapor temperature and pressure, and pressure rise times, detailed emplacement models can be developed by critical field and laboratory analysis of the resulting tephra deposits. Deposits left by dense flows of tephra and wet steam as opposed to those left by dilute flows of dry steam and tephra show contrasts in median grain size, dispersal area, grain shape, grain surface chemistry, and bed form.

Introduction

It was, perhaps, the 1883 eruption of Krakatau that triggered the geophysical awareness of the hydromagmatic eruption mechanism (Verbeek 1885). Volcanologists now widely recognize the importance of external water in explosive volcanism. Well-documented eruptions, such as Surtsey, Capelihnos, and Taal (Thorarinsson et al. 1964; Waters and Fisher 1971; Moore et al. 1966), have greatly increased our knowledge of activity associated with large-scale vaporization of lake and sea water by rising magma. Recently it has been shown that not only maars, tuff rings, and tuff cones (e. g. Womer et al. 1980; Sheridan and Wohletz 1981; Boivin et al. 1982), but portions of composite volcanoes and large ignimbrite sheets as well owe their existence to explosive hydromagmatic processes (e. g. Frazzetta et al. 1983; DeRita et al. 1983; Self 1983).

Hydromagmatic explosive behavior varies greatly, as do associated structures and deposits, and the circumstances under which magma contacts external water must be considered (e. g. Kokelaar 1983). Still, whatever mechanism is invoked to explain hydromagmatic eruptions, the phenomenon of water boiling is a fundamental problem. This phenomenon is complex in hydromagmatic systems because water generally is mixed with molten magma. Hence, a complex equation of state for the mixture arises and this is further complicated by dynamics of shock wave propagation. Recent work (e. g. Cronenberg 1980; Condiff 1982; Corradini 1981a) has concentrated upon developing fluid instability and detonation theories for the

rapid boiling process exhibited by interaction of molten metals with water, which are applied to experimental results for nuclear reactor, liquid natural gas, paper pulp, and metal smelter systems.

This paper summarizes some of the pertinent physical considerations of hydromagmatic eruptions. First, an idealized thermodynamic analysis shows the explosive potential of magma-water contacts, assuming that the two are intimately mixed. Secondly, the problem of how mixing occurs is discussed in the light of recent experimental studies of analog systems. Finally, a field example illustrates how geologic data can support a hydromagmatic hypothesis and be applied to obtain some theoretical understanding. Much of the first two parts of this paper attempts to be quantitative in description, since more graphical presentations have already been published.

Thermodynamic considerations

In the following discussion, it is shown how some predictions about magma-water interactions can be made from thermodynamics. Few now assume that nothing is known about the mechanism of the contact between magma and water, but that it results in production of high pressure steam that may explosively decompress. This assumption implies that thermal energy is transferred from the magma to the water as described by the second law of thermodynamics. The objective of this analysis is to find out how much work can be done by the explosive expansion of steam. Work is manifested in the fracture and excavation of country rock to form a crater, fragmentation of the magma into fine grained debris, and ejection of these fragments in an expanding jet of steam. For a hydrovolcanic eruption, it is necessary to find the work potential for expansion of the steam to atmospheric pressure. Calculation of the true potential requires determination of a complex set of boundary conditions unique to each volcano; but for simplicity and generality, one can make a few assumptions that allow analytical calculation of maximum potential.

For the system consisting of a mixture of magmatic particles and water and the surroundings being the volcano vent structure and the atmosphere, assume:

1. All the heat lost by the magma during the eruption is transferred to external water.
2. The liquid water and magma are incompressible, so that for each the specific heats remain constant with changing pressure and volume.
3. The specific volume of liquid water is small compared to that of its vapor.
4. The water vapor behaves as a perfect gas.
5. The volume of the magma does not change during the eruption (i. e. it does not vesiculate or contract during cooling).

All of these assumptions are more or less standard for a simple thermodynamic analysis. Certainly some heat is lost from the magma to country rock and the atmosphere during eruption, and magma does exhibit a finite volume change with quenching. Both of these may account for discrepancies of several percent. The other assumptions concern the exact thermodynamic properties of water. At supercritical states a deviation from ideality of 10% or more is expected, but since most volume change occurs at subcritical states for adiabatic expansion, the assumptions introduce very litle error into calculations, especially when extended or extrapolated steam table data (such as given by a modified Redlich-Kwong fit) are considered (Burnham et al. 1969; Holloway 1977; Kieffer and Delany 1979).

The Hicks-Menzies (1965) approach for this calculation was specifically formulated for molten melt-water interactions. It is generally considered to give maximum work potentials, and the illustration shown here is adapted from Oh (1985). The explosive interaction is considered to occur in two idealized stages (see Table 1 for definition of notation to be used). In the first stage, a mass of magma, m_m, at absolute temperature, T_m, somehow intimately mixes with a mass of external water, m_w, at absolute temperature, T_w, and thermal equilibrium is reached instantaneously. In the second stage, the system expands isentropically to atmospheric pressure, p_0, with a total change in the system's volume of ΔV_{sys}.

Thermal equilibrium stage

The first stage is described by the first law of thermodynamics as an adiabatic, nearly constant volume process where changes of potential and kinetic energy are neglected: $dU - dQ = dW = 0$, where dU is the change in specific internal energy of the system, dQ is the heat transport between the magma and water, and dW is the work output. Since the first stage is idealized as occurring at nearly constant volume (inside a confined region under the volcano or at such a rate that little vaporization occurs), heat of vaporization and consequently dW vanish. This law can be expressed more explicitly as:

$$m_w C_{vw}(T_e - T_w) + m_m C_{vm}(T_e - T_m) = 0 \quad (1)$$

where C_{vw} and C_{vm} are respectively the liquid water and magma specific heats at constant volume. If some expansion with vapor formation is allowed for this step, a term reflecting the internal energy of the vapor fraction and that required for vaporization should be included on the left-hand side of Eq. (1). This relationship allows estimation of the idealized equilibrium temperature, T_e. The equilibrium pressure, p_e, is estimated by assuming that the mixture can be modeled with a Redlich–Kwong equation of state:

$$p_e = \frac{RT_e}{(V_e - A)} - \frac{B}{T_e^{1/2}\ V_e(V_e + A)} \quad (2)$$

where R, A, and B are the gas constant, the covolume term

Table 1. Definition of notation

A	covolume term in Redlich-Kwong equation of state
B	attractive term in Redlich-Kwong equation of state
Bo	Bond number
Cd	coefficient of drag
C_p	specific heat at constant pressure
C_v	specific heat at constant volume
E	energy
E^*	total energy
J	nucleation rate of water vapor bubbles
KE	kinetic energy
Md	median diameter
PE	potential energy
Q	heat transport
R	universal gas constant (461.51 J $kg^{-1}K^{-1}$)
R^*	ratio of mass of water to that of melt
ΔR^*	$\lvert R^*_{max} - R^* \rvert$
S	specific entropy
T	temperature
U	specific internal energy
V	specific volume
W	work output
W_r	reversible work of equilibrium bubble formation
X	mass ratio effect number
Z	molecular collision rate per unit volume
a	water acceleration during vapor-film collapse
c	sound speed
g	gravitational acceleration
h	specific enthalpy
k	wave number
k_b	Boltzmann constant (5.6697×10^{-8} W m^{-2} K^{-4})
m	mass
n	time coefficient in Taylor solution
p	pressure
r	radius of vapor bubble
r_0	radius of melt fragments during coarse mixing with water prior to thermal detonation
r_1	radius of melt fragments after detonation
r'	pre-expanded vapor-film thickness
t	time
t_b	melt breakup time
t_v	velocity equilibrium time
t'	time span of Landau instability pressure pulse
u	velocity
x	steam mass fraction
α	thermal conductivity
ϕ	[$-\log_2$ (grain size in mm)]
Φ	phase
λ	wavelength
η	instability amplitude
κ	thermal diffusivity
ρ	density
σ	surface tension
σ_ϕ	Inman sorting coefficient
τ	characteristic time of instability growth

Subscripts

CJ	Chapman–Jouguet state
I	value for interface between water and magma
SN	value for spontaneous nucleation
c'	thermodynamic state at which water expansion goes from supercritical state to saturated state
$crit$	value at critical instability growth
d	themrodynamic state at which water expansion passes from saturated state to superheated state
e	value at equilibrium state
m	refers to property of melt (magma)
w	refers to property of liquid water
v	refers to property of water vapor
lv	refers to property at liquid-to-vapor phase transition
max	value at maximum conditions
mix	refers to property of melt and water mixture
rel	value of melt particles relative to that of water
ref	value at reference conditions
sys	value for system of magmatic particles and water
sur	value for surroundings, consisting of volcano vent structure and atmosphere
0	value at ambient conditions
1	value at initial state prior to interaction
2	value at final state after expansion to ambient pressure

(1.17×10^{-3}), and the attractive term (43961) for H_2O (SI units; Corradini 1981b). V_e is the equilibrium volume of the water, which can be taken as its initial volume.

The entropy of the equilibrium state, S_e, is solved from the definition: $dS = (C_v/T)dT + (\partial p/\partial T)_v \, dV$. For the simple, constant volume case in which vaporization does not occur, integration yields:

$$S_e = S_1 + C_v \ln(T_e/T_1). \tag{3}$$

Using steam tables, an alternative estimation of the pressure, p_e, for the first stage (equilibrium state) can be made. S_1 is about 300 kJ kg^{-1} K^{-1} ($T_1 = 298$ K), using the water triple-point as a standard state. If a small volume increase does occur, a third term is required for the right-hand side of Eq. (3), and it is equal to a constant (approximately 1.5 MPa/°C; Knapp and Knight (1977) multiplied by the expected volume change (in appropriate units). Then p_e and the steam fraction x_e can be calculated from saturated steam tables where:

$$x_e = \begin{cases} (S_e - S_l)/S_{lv}; & S_e \geqslant S_l \\ 0 & ; \ S_e < S_l \end{cases}$$

Subscripts l and lv refer to values for the saturated liquid and for vaporization of the saturated liquid at T_e. For supercritical equilibrium states, extended or extrapolated steam table data are required (see Kieffer and Delany 1979; Burnham et al. 1969).

Expansion stage

The expansion stage in which the system equilibrates to atmospheric pressure can be calculated for two "endmem-

ber" situations, which depend upon heat transfer to the steam during expansion. Using the terminology suggested by Self et al. (1979): the *adiabatic* case involves no heat transfer from pyroclasts, and the vapor expands isentropically; in the *isothermal* case—in which the two phases maintain a common temperature by perfect thermal contact and heat is continuously supplied to the vapor during expansion—the mixture behaves isentropically while the vapor increases in entropy. Maximum work potential is achieved for the isothermal case. Since the total energy, which is that of the System (E_{sys}) plus that of the surroundings (E_{sur}), is conserved during this stage, $\Delta E^*=0$, where by definition E^*=total energy, $\Delta E^*=\Delta E_{sys}+\Delta E_{sur}=0$, $\Delta E_{sys}=\Delta U+\Delta KE+\Delta PE$, and $\Delta E_{sur}=p_0\Delta V_{sys}$. In the definition KE is the kinetic energy, PE is the potential energy, and $p_0\Delta V_{sys}$ is the final state pressure times the volume change of the system. Since the work potential is defined as $-\Delta U$, the maximum work potential is given by $\Delta W_{sys}=\Delta KE+\Delta PE+p_0\Delta V_{sys}$. This maximum work expression takes into consideration that the internal energy partitioning into kinetic, potential, and expansion forms is not known, so it gives the maximum when in fact it is only the kinetic form that is readily observable during eruptions.

The system of the isothermal case consists of a mixture (*mix*) of magma and water, and the change in internal energy of this system ($-\Delta U_{mix}$) during expansion is the system work, which can be calculated as the sum of the changes in ΔU for the water and the magma: $\Delta W_{sys}=-\Delta U_{mix}=-\Delta(m_wU_w+m_mU_m)$. To evaluate the preceding equation, some arithmetic and some information from the steam tables can be used.

For the adiabatic case where the vapor separates from the pyroclasts prior to expansion, the thermal energy of the pyroclasts does not contribute and the vapor expands isentropically. The expansion calculation for this adiabatic case is straightforward and ΔW_{sys} (adiabatic) is simply $-\Delta(m_wU_w)$. For most explosive volcanic eruptions, vapor expansion is probably intermediate between isothermal and adiabatic. However, as pointed out by Self et al. (1979), the Strombolian endmember activity of hydrovolcanism is nearly adiabatic. Here, an example for the isothermal case is shown; the adiabatic case can be found in many introductory fluid mechanics texts. In this example analysis of expansion work is shown for both saturated and superheated steam.

Saturated state. Within the two-phase (liquid and vapor) region of the water phase diagram, the thermodynamic state for the mixture is

$$T_{mix}\mathrm{d}S_{mix}=\mathrm{d}h_{mix}-V_{mix}\mathrm{d}p_{mix}$$

where V is specific volume, the mixture enthalpy, h_{mix}, is defined as

$$h_{mix}=(m_wC_{pw}T+x\,m_wh_{lv}+m_mC_{pm}T)/(m_w+m_m), \quad (4)$$

and C_p is the constant pressure specific heat (w=water, m=magma), x is the mass fraction steam, and h_{lv} is the enthalpy required to convert saturated liquid water to saturated vapor. In order to find the steam mass fraction after the expansion, differentiate Eq. (4) to extrapolate values:

$$\mathrm{d}h_{mix}=\frac{(m_wC_{pw}+m_mC_{pm})\mathrm{d}T+m_wh_{lv}\mathrm{d}x}{m_w+m_m} \quad . \quad (5)$$

A simplified, ideal equation of state expression for the mixture volume is

$$V_{mix}=(x\,m_wV_{vw})/(m_w+m_m)=[(x\,R\,T)/p][m_w/(m_w+m_m)], \quad (6)$$

where V_{wv} is water vapor specific volume and R is the gas constant (461.51 J kg^{-1} K^{-1}). From the Clausius-Clapeyron relation find that

$$\mathrm{d}p_{mix}=(\mathrm{d}p/\mathrm{d}T)_{\text{sat. vapor}} \text{ and } \mathrm{d}p=(p\,h_{lv}\,\mathrm{d}T)/(R\,T^2). \quad (7)$$

The final mass fraction of steam, x_2, for this adiabatic, isentropic expansion can be found since the change in mixture enthalpy equals the volume of mixture times its change in pressure. So from Eqs. (4) through (7):

$$(m_wC_{pw}+m_mC_{pm})\,\mathrm{d}T/T-m_wh_{lv}\,\mathrm{d}(x/T)=0.$$

This expression can be integrated between the equilibrium (e) and final states (2) and rearranged to give x_2:

$$x_2=T_2\left[\frac{x_e}{T_e}+\frac{(m_wC_{pw}+m_mC_{pm})}{m_wh_{lv}}\ln\left(\frac{T_e}{T_2}\right)\right]. \quad (8)$$

Superheated state. Now consider expansion of the water in a superheated state, first by defining the change in mixture enthalpy as:

$$\mathrm{d}h_{mix}=\frac{(m_wC_{pv}+m_mC_{pm})\mathrm{d}T}{m_w+m_m} \quad , \quad (9)$$

where $C_{pv}$is the specific heat of the water vapor at constant pressure. Since x=1.0, the mixture volume is

$$V_{mix}=(R\,T/p)\,[m_w/(m_w+m_m)]. \quad (10)$$

Again using the Clausius-Clapeyron relation, find that

$$\mathrm{d}p_{mix}=\mathrm{d}p_{vapor}. \quad (11)$$

So by assuming that the change in mixture enthalpy equals the change in the vapor pressure times the mixture volume, one obtains from Eqs. (9) through (11):

$$\frac{(m_wC_{pv}+m_mC_{pm})}{m_wR}\frac{\mathrm{d}T}{T}=\frac{\mathrm{d}p}{p} \quad ,$$

which can be integrated from the saturated vapor state (x=1) or superheated state to the final superheated state to give the final temperature, T_2:

$$T_2=T(p_2/p)^{1/f} \quad (12)$$

where $f=(m_wC_{pv}+m_mC_{pm})/m_wR$, and T and p are taken at the equilibrium state or that point on the saturation curve (T_d) where the expansion passes from the two-phase region to the vapor region.

Calculation of the expansion work

Depending upon the amount of water contacting magma, the equilibrium state produced during the initial mixing may be at a pressure and temperature ranging from sub- to supercritical conditions. Accordingly, the expansion stage may take the water through one of several thermodynamic pathways within either or both of the saturated (two-phase) and superheated (vapor-phase) regions. The actual pathway involved for any one system is strongly a function of the water-melt mass ratio because it determines the equilibrium state for an idealized system. Four pathways are shown in Fig. 1, a temperature-entropy diagram for water, where the equilibrium states (e) and final states (2) are shown. Of the four pathways, path 1 (entirely in the saturated region), path 2 (saturated to superheated), and path 4 (supercritical and superheated) can be quantified as to work potential from the above equations. For path 3 (superheated to saturated), point c' must be found where the path crosses from the supercritical (superheated) to the saturated region left or right of the critical point (Fig. 1). This path can be calculated as a combination of paths 1 and 4 with $x=0$ for crossing on the left side and $x=1$ for the right side of the critical point. Note that for the right side of the critical point c' must satisfy the condition given in Eq. (12). Diagrams from Kieffer and Delany (1979) are helpful in this analysis.

As an example, consider point d (Fig. 1) where path 2 crosses from the saturated to the superheated region during some hypothetical expansion. The system work is evaluated by:

$$\Delta W_{sys} = -\Delta U = -\Delta(m_w U_w + m_m U_m) = m_w[C_{vw}(T_e - T_d) + x_e(h_{lv} - p\,V_{lv})_e - x_2(h_{lv} - p\,V_{lv})_2] + m_m C_{vm}(T_e - T_d) + (m_w C_{vv} + m_m C_{vm})\,(T_d - T_2),$$

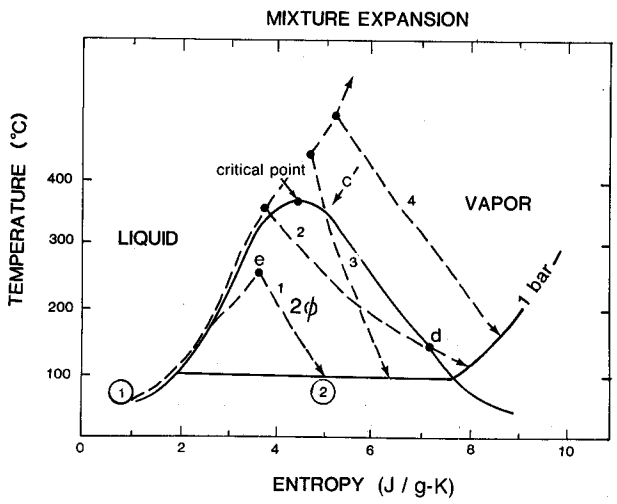

Fig. 1. Temperature versus entropy diagram for water in the *isothermal* case where the mixture of water and pyroclasts isentropically expands. Four possible pathways are shown; see text for description (2Φ=vapor and liquid). Note that for the mixture expansion, vapor entropy always increases for the isothermal case, which can be contrasted to the adiabatic case, not shown here, in which vapor expands isentropically

where T_d is the temperature for $x=1$, C_{vv} is the specific heat of water vapor at constant volume, and the subscripts lv designate values for the phase change. Now the efficiency, defined as the system work divided by the magma's thermal energy, is often termed the conversion ratio (CR), because it includes not only the amount of heat energy converted to kinetic energy but also the amount of the potential energy and $p_0\Delta V$ in the system:

$$\text{Efficiency} = CR = \frac{\Delta W_{sys}}{m_m C_m (T_m - T_{ref})} = \frac{\Delta KE + \Delta PE + p_0 \Delta V_{sys}}{m_m C_m (T_m - T_{ref})}, \quad (13)$$

where the denominators represent the thermal energy of the magma, using 298 K as a reference temperature. This efficiency or conversion ratio of thermal energy to mechanical work is a convenient number by which to express a volcano's explosive energy where the erupted volume is known and an approximate mass fraction of water involved can be estimated. In the event that the water mass fraction cannot be easily estimated, as is generally the case for many volcanic systems, one can use deposit characteristics, such as grain size (reviewed by Sheridan and Wohletz 1983), as an estimate of the water-magma mass ratio.

For any melt-water explosion it is likely that only a small percentage (10% or less) of the magma's heat gets converted to explosive energy, because mixing of the magma and water does not achieve the state of completeness required by the ideal model given above. If mixing did reach the theoretical limits for complete thermal equilibrium, which requires melt fragmentation to approximately 1 μm (Wohletz 1983a), one would expect deposits to be uniformly extremely fine grained with all juvenile particles several micrometers or less in diameter. Although some phreatomagmatic deposits exhibit strong fragmentation with median diameters in the range of several tens of micrometers, most finer material is carried to distal localities in atmospheric suspension. In that case, it is difficult to determine what portion of magma achieved complete fragmentation and thermal equilibrium with external water. The typically polymodal, log-normal size distribution of phreatomagmatic deposits is a measure of what portion of erupted magma experienced intimate mixing and approached thermal equilibrium with external water.

In conclusion to this section, Fig. 2 illustrates some results of the above thermodynamic calculation for a constant ambient pressure expansion of an isentropic mixture of magma fragments and steam (isothermal case). If the steam quickly separates from the magma fragments and thermal equilibrium between the pyroclasts and steam is not maintained during the isentropic expansion, then smaller efficiencies are reached (adiabatic case). As was mentioned earlier, most hydrovolcanic explosions probably exhibit behavior in between adiabatic and isothermal.

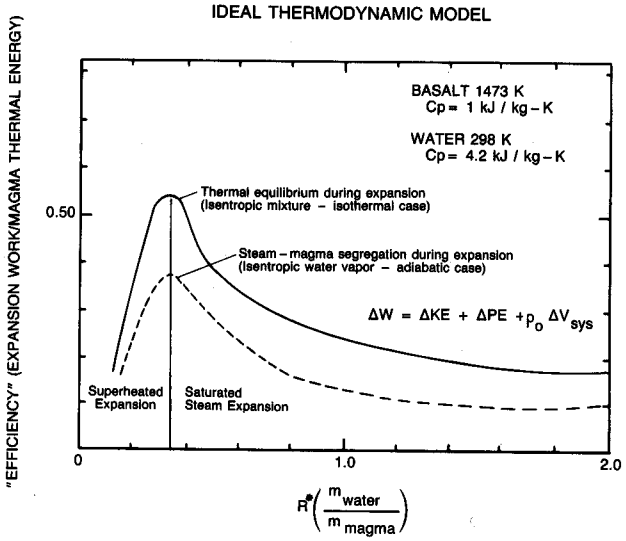

Fig. 2. Results of the thermodynamic calculation show the dependence of thermodynamic efficiency upon R^*, the mass ratio of water to magma. Two curves are shown, one for the isothermal case and the other for the adiabatic case. Those pathways shown in Fig. 1 that are predominantly in the 2Φ region will result in saturated or wet steam production

In ballistic ejection, pyroclasts quickly separate from enclosing steam, but in surge transport steam moves along with the pyroclasts. In the surge case, much of the steam may segregate from the surge, rising above it, leaving dry deposits that exhibit only small amounts of condensed vapor. On the other hand, much steam may condense during transport in surges, resulting in wet deposits. Hence, in addition to the initial mass ratio of water and magma, which determines the theoretical efficiency, the mode of expansion and tephra transport determines whether the adiabatic or isothermal maximum is approached. The aim of field work is to evaluate the water-magma ratio and probable mode of tephra transport so that relative explosive potentials can be constrained. Note that in the case where depositional stages of the eruption are considered, the "total work" done by the explosion is integrated over many seconds. Comparison of instantaneous explosive energy should involve the time derivative of energy, which is power.

Mechanisms of magma-water mixing and explosion

A qualitative discussion of the mechanisms by which magma and external water intimately mix, resulting in the large-scale heat exchange discussed above, has been given by Wohletz (1983a). Although there are numerous mixing models described in literature, recent work points to just two theories that satisfactorily explain most explosions that occur during the contact of a hot fluid with a cold one (fuel-coolant interaction, FCI). FCI is such a general physical process that it includes phenomena ranging from passive quenching, permitted by insulating steam envelopes, to dynamic explosions resulting from instability of film boiling interfaces. The theories for explosive behavior are the spontaneous nucleation (superheating) model and the thermal detonation model. Both models require that a period of film boiling should occur prior to explosion. Film boiling permits two processes to occur simultaneously: partial thermal insulation of the molten magma from the water, and gradual fragmentation and mixing of the magma with water by the instabilities arising from film boiling. With the increased area of heat transfer caused by mixing, rapid vaporization and explosion occur according to theory if (1) water is superheated to the temperature of spontaneous (homogeneous) vapor nucleation; or (2) an externally generated pressure wave (trigger) propagates with sufficient strength to cause fine fragmentation and collapse of insulating film barriers around fragments, resulting in rapid heat transfer and vapor production. The following discussions attempt to illustrate somewhat quantitatively the basic features of these two mechanisms.

Superheating

The superheat limit case (Fauske 1973) requires that during the contact of hot magma with water, the interface contact temperature (T_I) be above the spontaneous nucleation temperature (T_{SN}) of the water. Heterogeneous boiling in pure water occurs at any given pressure below the critical point when the temperature is above the equilibrium boiling temperature (373 K at sea level and increasing to 647 K as pressure increases to critical values near 22.0 MPa). The effect of dissolved solids, such as that found in sea water, can increase the pressure and temperature of critical behavior (e. g. to nearly 40 MPa and 720 K as NaCl concentration approaches 5 wt.% in water; Sourirajan and Kennedy 1962). Superheating refers to a metastable thermodynamic state where, for this case, water remains in the liquid state above its boiling temperature for any given pressure. In this condition, any one of many different physical or chemical disturbances can trigger water to flash into steam. For example, the sharp jarring of a body of metastable water by a moderate-to-high-frequency seismic wave might cause localized entropy changes of sufficient rapidity to initiate a nucleate boiling front that propagates as a vaporization wave. Even without external triggers, superheating can only progress to a maximum temperature, T_{SN}, before spontaneous vaporization occurs by homogeneous boiling. This case of vapor explosion is to be expected when water is heated so rapidly that it reaches T_{SN} before external triggers cause vaporization.

The limiting case for vapor explosion can be easily calculated: $T_I > T_{SN}$ where:

$$T_I = \frac{T_m[\alpha/(\kappa)^{1/2}]_m + T_w[\alpha/(\kappa)^{1/2}]_w}{[\alpha/(\kappa)^{1/2}]_m + [\alpha/(\kappa)^{1/2}]_w} \quad , \tag{14}$$

and T = temperature, α = thermal conductivity, κ = thermal diffusivity (α/C_v, where C_v is the heat capacity at constant volume), m = molten material, and w = water. For basalt at 1473 K, α_m=2.1 J m^{-1} s^{-1} K^{-1}, and for water at 298 K, α_w=0.61 J m^{-1} s^{-1} K^{-1}; the SI value of $\alpha/(\kappa)^{1/2}$ for the basalt is about 2297, and it is 1596 for water; these conditions set T_I at about 990 K. The spontaneous nucleation temperature, T_{SN} (Fig. 3), is given by the kinetic theory rate equation (Frenkel 1946): $J=Z$ exp $(-W_r/k_bT)$, where T_{SN} occurs at T satisfying the condition:

$$dJ/dT \cong 10^{15} \cong (Z\, W/k_bT^2) \exp(-W_r/k_bT).$$

For the rate equation J=rate of bubble nucleation per unit area, Z is a constant characterizing the molecular collision rate per unit volume (about 10^{40} m^{-3} s^{-1} for water), k_b=Boltzmann's constant (5.6697×10^{-8} W m^{-2} K^{-4}), and W_r is the reversible work of equilibrium bubble formation in the liquid, which is $W_r=16\ \pi\ \sigma^3/3(p_v-p_l)^2$, where σ=surface tension of the pure liquid, and p_v and p_l are the vapor and liquid pressures respectively. The bubble work function is dependent upon the contact wetting angle, which is important for impure liquids and results in somewhat lower values of T_{SN}. For water, the highest value of superheating attained in the laboratory is around 563 K, which is about 20 K less than that predicted by the rate equation, but this value theoretically increases with pressure towards that of the critical point (Reid 1976). For most experimental conditions $T_{SN}\cong$570 K. Results for Eq. (14) show that the requirement of superheating is easily met for the initial conditions of basalt-water contact. Note that the wetting angle may be less on liquid magma surfaces than on those of solidified magma.

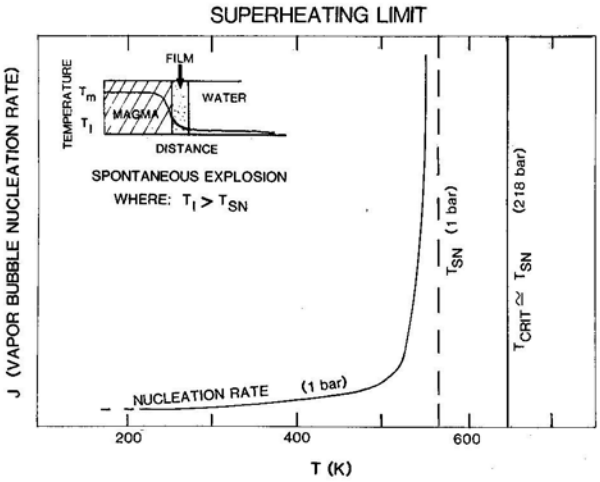

Fig. 3. Illustration of the superheating limit criteria for vapor explosion. As the interface temperature approaches that of the spontaneous nucleation temperature T_{SN}, the vapor bubble nucleation rate increases exponentially to the point at which vapor production occurs at explosive rates

Experiments on FCIs (Buxton and Benedict 1979; Nelson and Duda 1981; Froehlich et al. 1976) have shown that once a vapor film has formed by coalescence of many small bubbles at the melt-water interface, the film oscillates in thickness. The oscillating film may remain hydrodynamically stable and serve as insulation between the liquid water and magma. Hence the two phases may remain in contact without explosive heat transfer while coarse mixing occurs. The oscillations can occur rapidly on a microsecond to millisecond scale, and as more heat energy is transferred to the film, the density differences among the film, liquid water, and melt become sufficient to cause growth of fluid instabilities. These instabilities can effectively cause the magma and water to intimately mix, forming a slurry. If this type of bulk mixing occurs before the superheat limit is achieved, large volumes of magma and water can contribute to explosions. On the other hand, if the superheat limit is reached prior to instability-driven mixing, explosions may occur at interfaces, involving only limited volumes of magma and water.

Several instability types are considered to be important in bulk mixing of magma and water. The Landau instability (Shepherd and Sturtevant 1982; Sturtevant and Frost 1984) occurs during the bubble film growth phase. Vorticity produced at the vapor-liquid interface by evaporation causes roughening of that interface to the point where the liquid becomes fragmented. The Taylor instability (Corradini 1981a) grows during collapse of the film because of the large acceleration normal to the melt-water interface; this instability also can distort and fragment the melt surface. The result of interfacial roughening and tearing is production of melt particles where the amplitude of the instability has exceeded the amount allowed by the melt's surface tension. The Kelvin-Helmholtz instability (Berman 1984; Berenson 1961) produces similar results if accelerations of the water are parallel to the magma interface. However, growth of the Kelvin-Helmholtz instability is important mainly for systems where there are small density differences and may not be important except for strongly vesiculated magma. Although growth of these instabilities is limited by the time scale of vapor oscillation, many experimental studies show that they do occur rapidly enough effectively to mix large volumes of melt and water prior to explosion.

Of these instability types the Taylor mechanism is perhaps the best studied, and it serves to illustrate the idea of fluid instability mixing (Fig. 4). From solution of the momentum equation (Bellman and Pennington 1954), the Taylor instability can be shown to grow with time, t, as in the case of a planar contact of incompressible fluids where the contact is initially perturbed: η=cosh (nt), in which

$$n=\left[\frac{a(\varrho_m-\varrho_w)k}{\varrho_m+\varrho_w}-\frac{\sigma k^3}{\varrho_m+\varrho_w}\right]^{1/2},$$

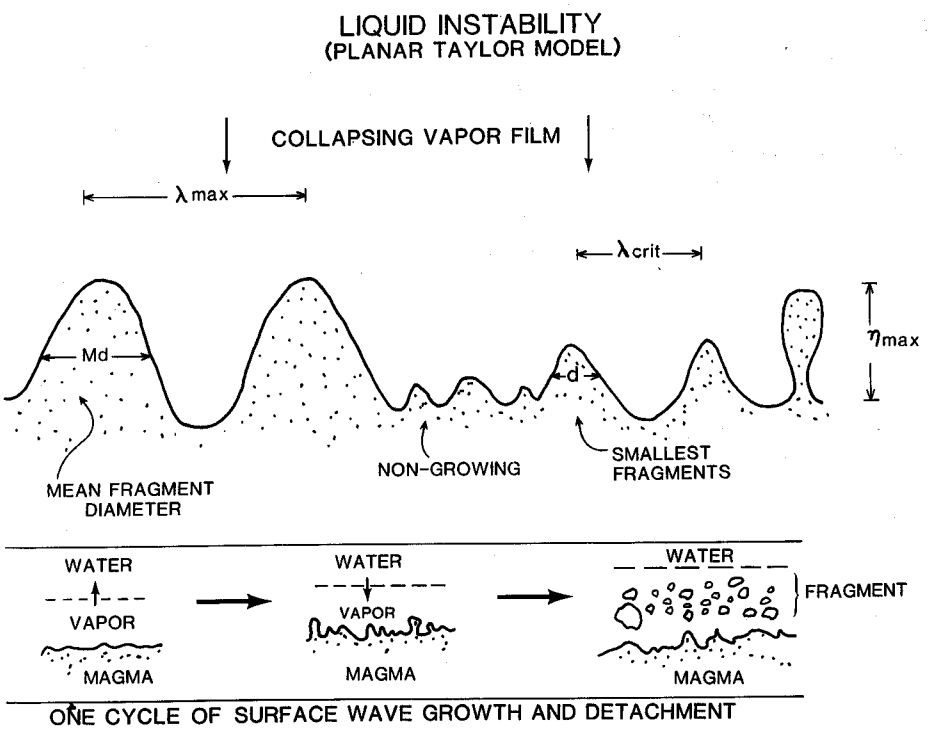

Fig. 4. Illustration of a planar Taylor instability at the interface between magma and a collapsing water-vapor film (*top*). A complete cycle of instability growth is shown at the bottom (see text for description). Oscillation of the film thickness transmits sufficient momentum to the magma so that its surface distorts into waves that can grow until they detach to form small fragments

and η is the instability amplitude, a is the acceleration of nearly incompressible water (and condensing vapor film) towards the melt surface during film collapse phases (100 $g < a < 1000\ g$ for analogous systems; Corradini 1978), P is the density of the water (w) and melt (m), k is the instability wave number (2π/wavelength), and σ is the melt surface tension ($\sigma \cong 0.35$ N m^{-1} for basalt melts of $\rho_m \cong 2.7 \times 10^3$ kg m^{-3}; Williams and McBirney 1979). However, for an initial disturbance to grow in amplitude without damping out, its wavelength, λ, must be greater than a critical value, λ_{crit}:

$$\lambda_{crit} = \left[\frac{2\pi}{k_{crit}}\right] = 2\pi\left[\frac{\sigma}{a(\varrho_m - \varrho_w}\right]^{1/2}.$$

A whole spectrum of possible λ may grow, but the fastest growing one (inviscid case), λ_{max}, is given by:

$$\lambda_{max} = \left[\frac{2\pi}{k_{max}}\right] = 2\pi\left[\frac{3\sigma}{a(\varrho_m - \varrho_w)}\right]^{1/2} = 3^{1/2}\lambda_{crit}. \qquad (15)$$

Since λ_{max} forms most quickly, magma fragments resulting from it will be more abundant than those resulting from other wavelengths. For the case of explosive mixing of magma with water, $\lambda_{max}/2$ can be considered as approximately the median grain diameter of tephra produced. This type of fragmentation may be expected to produce irregular, bulbous, mossy, and nearly spherical clast shapes (Types 3 and 4 of Wohletz 1983a). The characteristic growth time, τ, of the Taylor instability can be calculated by:

$$\tau = \frac{1}{n_{max}} = \left[\frac{3(3\sigma)^{1/2}(\varrho_m - \varrho_w)}{[a(\varrho_m - \varrho_w)]^{3/2}}\right]^{1/2}, \qquad (16)$$

so that λ_{max}/τ is a measure of average speed by which this mixing phenomenon may propagate from the initial contact surface towards the interior of an extruding mass. A similar set of relationships can be derived for the Kelvin-Helmholtz instability (Chandrasekhar 1968) in which the relative velocity of the water to the melt is considered in place of acceleration.

Equations (15) and (16) have proved to be useful in predicting particle size and mixing times for experimental melt-water interactions (Corradini 1978; Berman 1983). In predicting thermite-water interactions, the calculated mean particle diameters ($\lambda_{max}/2$) are smaller than several millimeters, and instability growth occurs in characteristic times less than several milliseconds. These calculations agree well with experimental results. As a simple application to a geologic example, consider a 10-m-wide dike intruding near-surface, water-saturated sediments. Individual hydromagmatic explosions are predicted to produce ash- to lapilli-sized fragments, and to show explosive pulses lasting up to several seconds or more, the time needed for the mixing to occur.

Bellman and Pennington (1954) investigated the effects of surface tension and viscosity on the Taylor instability.

Surface tension controls the size of fastest growing wavelengths (Eq. (15)), and since laboratory-measured surface tensions decrease with increasing silica content of lavas (Williams and McBirney 1979), one might expect rhyolitic hydrovolcanic products generally to be finer grained than their basaltic counterparts, which is a trend noted by Sheridan and Wohletz (1983). Viscosity, on the other hand, reduces the growth rate of the instability. Hence, for strong interaction with water to occur, viscous magmas require longer mixing times than fluid ones. So it is, therefore, logical to conclude that when all other factors such as vesicularity and vent size are equal, rhyolites are less prone than basalts to interact explosively with water.

Of the instability mechanisms that promote superheat vapor explosions, the Landau instability (Shepherd and Sturtevant 1982) may best fit experimental observations because it not only promotes large heat transfer rates but also describes the large mass fluxes observed for many FCIs. The Landau mechanism requires geometrical constraints that determine whether mass fluxes and accelerations in a melt-water system are susceptible to instability growth. For this reason, modeling of the Landau instability allows prediction of those interaction situations most likely to be explosive. However, the details of applying this mechanism have yet to be fully developed in a general manner.

An important aspect of superheat vaporization, the suppression of bubble growth by pressure, is predicted by a form of the Rayleigh bubble-growth equation:

$$\frac{du}{dt}=\frac{1}{r}\left[\frac{(p_f-p_{amb})}{\varrho}-\frac{3}{2}u^2\right],$$

where the outward acceleration of a bubble surface du/dt depends upon the bubble radius r, with p_f and p_{amb} being the vapor pressure and ambient pressure respectively, and ρ the liquid density. Predictions based upon the above consideration put the pressure threshold for spontaneous nucleation at about 1.3 MPa (Henry and Miyazaki 1978). Above that pressure superheating vapor explosions are supposed to be improbable. This limit is equivalent to about 50 to 100 m depth of bural (130 m depth in sea water) for basalt-water interactions. Sturtevant and Frost (1984) show that the pressure suppression effect is especially true for the Landau instability. It seems clear that other processes must play a role for explosions to initiate at greater depths.

The drawback to the spontaneous nucleation (superheating) model is that it does not strictly fit experimental data at higher pressures. Volcano experiments (Wohletz and McQueen 1984) have shown that violent FCI explosions occur at confining pressures greater than 35 MPa. Since the scaling relationships for FCIs are incompletely understood, there is yet a strong possibility that scale may be critically important in determining the type of fluid instability that may evolve at the fuel-coolant interface. Small (<1 kg) interactions appear to be limited to a superheating type of interaction (Taylor and Landau instabilities) whereas large ones (i. e. volcanic) may support a "detonation" type of interaction. This consideration has led other workers (e. g. Board et al. 1975; Patel and Theofanous 1978; Condiff 1982) to consider that this mechanism may cause explosions in fuel-coolant systems at higher ambient pressures, as is discussed in the following section.

Thermal detonation

Unlike chemical detonations, which are gas-evolving chemical reactions driven at high pressure and high temperature by a propagating shock wave, a thermal detonation only entails rapid vaporization of a liquid behind a propagating shock. Thermal detonation has been called "polymorphic detonation," referring to rapid phase change (Rabie et al. 1979; Fowles 1979). The analysis of this mechanism requires the assumption that fragmentation and intermixing of the melt with the water are not controlled by vapor bubble nucleation but rather by the rapidly changing pressure-volume conditions existing across a shock wave moving through the melt-water mixture (Fig. 5). In this model, an externally generated shock wave causes a differential acceleration of melt particles relative to the water. This acceleration has been found, based upon shock tube experiments on melt-water systems (Sharon and Bankoff 1981), to cause breakup of the melt into finer particles with rapid thermal equilibration occurring in the expanding region behind the shock. If the vapor expansion caused by thermal equilibration of finely divided melt particles surrounded by water is great enough to produce particle velocities satisfying the Chapman-Jouguet (*C-J*) condition (a thermodynamic state in which resulting hydrodynamics are those of detonation; Courant and Friedrichs 1948), the shock wave will be sustained. In order to meet the requirements of the *C-J* condition, the melt breakup time (t_b) must be shorter than the time needed for velocity equilibration, t_v (the point at which melt particles and water have reached the same velocity). This requirement has been found to be adequately expressed as a function of the Bond number (*Bo*).

$$t_b/t_v=\frac{3\,\rho_w C_d X}{8\rho_w(\rho_m/\rho_w)^{1/2}}\,44\,Bo^{-1/4}<1. \qquad (17)$$

This equation, derived by Fauske (1977), has been modified in a manner similar to that suggested by Bankoff and Jo (1976) so that it includes the water-to-melt mass ratio effect, X. The coefficient of drag (C_d) on melt particles suspended in water has been assumed to be about 2, but Fauske (1977) showed that for numerous particles closely packed in a matrix of water, C_d is more realistically about 68. This variation of C_d can be accounted for by X, a function of water-to-melt ratio. For work with experimental volcano

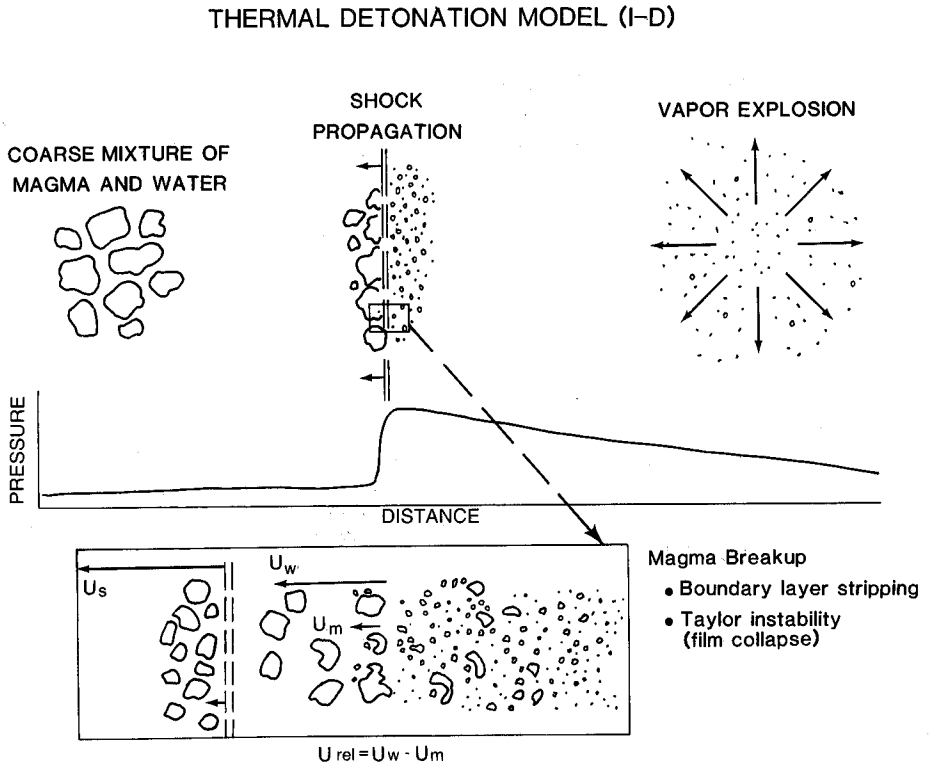

Fig. 5. An alternative model of strong magma–water interaction followed by explosion requires the propagation and sustenance of a shock wave as a *thermal detonation*. The *inset box* shows an expanded view of conditions across the shock wave where u_s is the shock velocity, u_w is the water velocity, and u_m is the magma fragment velocity. Where $u_{rel}=u_w-u_m$ reaches a large enough magnitude, magma breakup by processes such as boundary layer stripping and Taylor instability may result in large heat transfer rates

systems, it has been useful to empirically fit X to experimental results:

$$X=(0.1\ R^*_{max}/R^*)\ [\exp\ (\Delta R^*)]$$

where R^* and R^*_{max} are the water-to-melt mass ratio and optimum observed explosive ratios respectively, and ΔR^* is the absolute value of $R^*_{max}-R^*$ (Wohletz and McQueen 1984). With this expression, one can make some predictions about the explosive potential of magma-water systems.

Rewriting Eq. (17) with appropriate density values and X, a simple dimensionless expression is obtained,

$$280\ X\ Bo^{-1/4} < 1,$$

for a "detonation" model for phreatomagmatic explosions. The Bond number, a measure of the tendency of a fluid to break up during acceleration, is 3/8 the product of the coefficient of drag (C_d) and the Weber number (a ratio of inertial forces to surface tension forces). The Bond number is given by:

$$Bo=\frac{3\ \rho_w\ u_{rel}^2\ r_0\ C_d}{8\ \sigma} \qquad (18)$$

where u_{rel} is the melt–water relative velocity caused by passage of the shock, r_0 is the initial melt particle radius, and σ is the melt surface tension. u_{rel} is determined by mass and momentum conservation across the shock, assuming Rankine–Hugoniot conditions and knowing initial p_{init} and V_{init} of the mixture and the p and V of the shocked material. For detonation u_{rel} is found for the p and v at the *C-J* plane where the velocity of the material leaving the shock front is just sonic with respect to the front (a necessary requirement for a stable, self-sustaining explosion; Landau and Lifshitz 1959):

$$u_{rel}=[(p_{CJ}-p_{init})\ (V_{init}-V_{CJ})]^{1/2}.$$

Board et al. (1975) estimated $u_{rel} \cong 100$ m/s^{-1}. Corradini (1981b) estimated u_{rel} as $u_{rel}=(p-p_0)/\rho_w c_w-(p-p_0)/\rho_m c_m$.

For volcano experiments, $\rho_w=1\times10^3$ kg/m^3, $c_w\cong1.5\times10^3$ m/s, $\rho_m=4\times10^3$ kg/m^3, and $c_m\cong5\times10^3$ m/s. These conditions allow prediction of u_{rel} at about 60 m/s for satisfaction of the *C-J* requirements of $p\cong100$ MPa for $p_0=0.1$ MPa. Increasing p_0 (decreasing V_{init}) increases the value of pressure at the *C-J* plane, which can decrease the likelihood of attaining detonation. These values also agree with Drumheller's (1979) numerical calculations based upon collapse of a vapor film around a molten metal drop. If relative velocities produced are lower than the $\cong$60 m/s needed to sustain detonation, then the explosion will be quickly damped. Accordingly a critical Bond number must be exceeded by the system in order to maintain a detonation where:

$$Bo_{crit}=\frac{Bo}{3\ X}\quad[(p_{CJ}-p_0)/p_{CJ}]^2$$

as empirically determined from volcano experiments where p_{CJ} is taken at 100 MPa. Thus the mass ratio and ambient pressure effects have been included to fit experimental data and the relative velocity can be calculated:

$$u_{rel}=(8\sigma Bo_{crit}/3\rho_w r_0 c_d)^{1/2} \quad (19)$$

from the definition of Bo given in Eq. (18). The radius r_1 of melt particles caused by the shock breakup is approximated from data as:

$$r_1=(8\ \sigma/\rho_w u_{rel}^2)\ 10^2\Delta R^*. \quad (20)$$

Figure 6 illustrates for various mass ratios the calculated u_{rel} and r_1 showing the threshold for detonation at mass ratios greater than 0.2 and less than or equal to about 4.0 at p_0=0.1 MPa. The limiting effect of increased ambient pressure also shown in Fig. 6 indicates that detonating interaction is not likely to occur much above a p_0 of 50 MPa (500 bars). Without considering the mass ratio effect, Fauske (1977) argued that very large r_0 values (r_0>10 m) are needed to satisfy the Bo_{crit} of 10^4cited by Board et al. (1975) as necessary for *C-J* conditions to exist in melt-water systems. Irrespective of the mass ratio arguments shown above, volcanic systems can satisfy detonation requirements, whereas smaller single 1-gram-drop laboratory experiments may not.

Discussion of thermodynamic and hydrodynamic models

The above discussions illustrate some quantitative approaches to understanding the hydromagmatic explosion mechanism. The detailed description of how water and magma mix and explosively interact will certainly change as more is learned about this problem. Considerations of thermodynamics and mixing mechanisms place some constraint on the interpretation of important field parameters. For example, partitioning of the magma thermal energy into kinetic energy of ejection can be described by basic thermodynamic principles, which allows us to make some judgment on the potential danger of a given eruption. The hydrodynamics of magma fragmentation by explosive contact with water also place constraints on particle sizes produced and depth of interaction. Together, these descriptions facilitate intepretation of field measurement of tephra deposit thicknesses, bed forms, and grain sizes (shown above) and judgment of emplacement wetness.

Consider the limitations and weaknesses of the hydrodynamic models: for the superheating (spontaneous nucleation) explanation, superheating is not clearly observed in experiments; no criteria are included for the mass ratio effects; vapor explosions have been experimentally observed for situations in which T_I was not greater than T_{SN} and for others in which T_I was much greater than T_{crit}; the suppression effect of increased ambient pressure

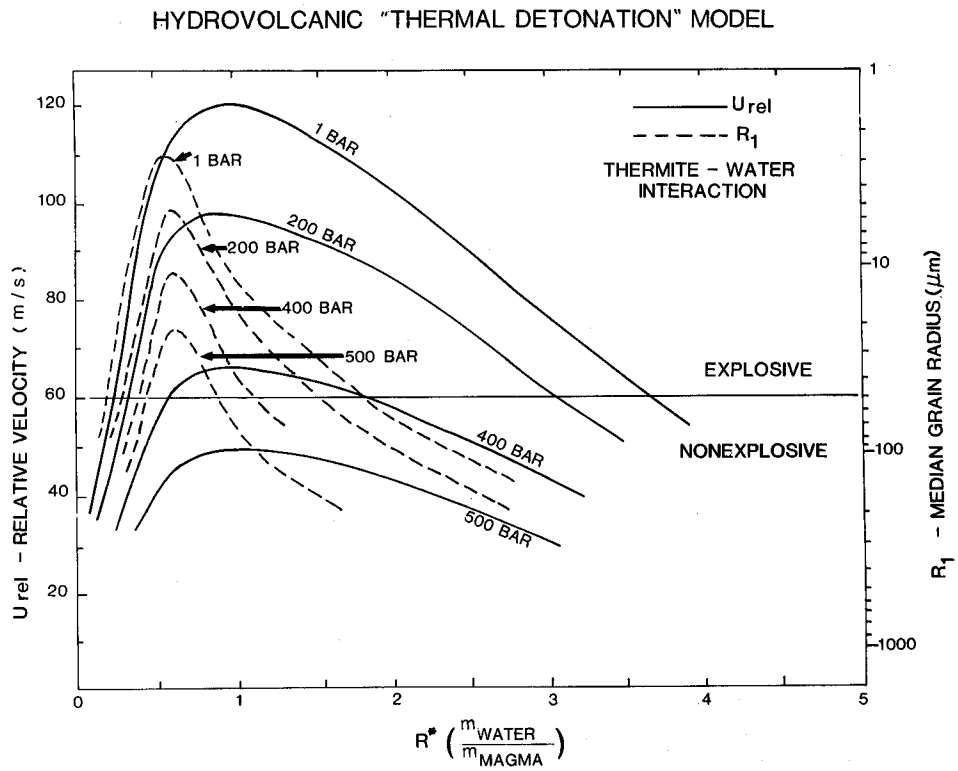

Fig. 6. Application of the thermal detonation model illustrated in Fig. 5 allows calculation of relative velocity u_{rel} of magma fragments to water in the slurry. If u_{rel} increases beyond about 60 m/s, then magma breakup can occur resulting in high heat transfer rates and subsequent vapor explosion. Note that u_{rel} for the explosive-nonexplosive boundary may vary by plus or minus several tens of meters per second depending upon rheological properties of the melt. *Solid lines* show the dependence of u_{rel} upon R^* for different ambient pressures. The degree of magma breakup determines the resulting tephra grain sizes, r_1, and these are shown as *dashed lines*

has not been clearly documented (vapor explosions can be triggered at much higher pressures than supposed suppression limits); and the effect of varying melt rheology and crystallization is poorly understood. For the thermal detonation model, although it appears to be experimentally verified, a large trigger (pressure wave) might be required to initiate the event; the actual mechanism by which fragmentation is achieved behind the shock is poorly understood; the theory of a Chapman-Jouguet detonation wave was developed for single-phase, chemical reactions; shock waves in two-phase flow are not well understood; and the dispersion effect that a heterogeneous mixture has upon a shock wave together with lateral slip velocities behind the shock may prevent attainment of detonation.

The geometry of the initial contact between magma and water will not be discussed in detail. This important consideration covers aspects such as dike intrusions, spilling of lava on the bottom of a body of water, enlargement of a region of subsurface magma-water interaction by explosive excavations, and entrapment of water in a lava tube. The contact area that results from various geometries and variation of its size with time can be modeled by close observation of available geologic exposures in vent areas. This exercise is especially rewarding in eroded vent localities. Kokelaar (1982) shows some examples for intrusive bodies, Wohletz and McQueen (1984) give an example for dike intrusion of wet sediments, and Froelich et al. (1978) describe experiments of water entrapment in molten metals.

Melt granulation by thermal stress resulting from quenching (Carlisle 1963) has not been discussed because present research into FCIs indicates that it does not greatly contribute to large vapor explosions (Ladisch 1977). However, where quenching does create stresses large enough to initiate large explosions, the process may proceed as a thermal detonation, which may produce angular, blocky particles. Quenching may transmit added heat energy to water over small temperature changes because of the finite fusion enthalpy of some melts. One of the perhaps more interesting applications of the calculations presented here is for predicting the stress required to fracture lavas. Fisher (1948) shows that for fluid liquids, fracture occurs by bubble nucleation when a negative pressure pulse exceeds the equilibrium vapor pressure of the fluid. A form of the bubble formation and work equations shown above can be applied in this analysis where dissolved volatiles are present in the melt (see Burnham 1983). For failure of viscous liquid by nucleation and propagation of cracks, Fisher (1948) also uses a nucleation and work equation for prediction of fracture stress. Surface tension is the dominant material property for fluid fracture, but for viscous fracture Young's Modulus and Poisson's Ratio are also necessary for analysis. So, depending upon the degree of magma cooling before fragmentation, either brittle, curviplanar fracturing or vesicular fragmentation may dominate clast morphology. Glass near the transition temperature from liquid to solid behavior may fracture by both mechanisms (provided there is a volatile material in the glass) when subjected to strong pressure waves propagated from regions where vapor explosions occur.

The problem of the depth at which water and magma explosively interact was well documented by Heiken (1971). Data from Pike and Clow (1981) plotted in Fig. 7 show crater depths of tuff rings and tuff cones, measured over much of the earth's surface from satellite imagery (Crowe et al. 1985). Assuming that the crater floor of these landforms is an indication of the level of steam explosion (Self et al. 1980), one finds that the mean depth of explosion for the cases considered is about 91 ±67 m, and that the maximum depth is nearly 400 m, roughly equivalent to about 9.8 MPa of initial overburden pressure ($\rho=2.5\times10^3$ kg/m^3). One might conclude that confining pressure is an important limit to explosive water-magma interaction. However, it appears possible, based on the detonation model, that the intermixing of ground water with magma can lead to explosions and that the actual depth of explosion is limited only by the strength of the surrounding country rock. This latter concept is supported by the analysis of eruptions at Vesuvius (Sheridan et al. 1981) where the aquifer depth is as deep as 5 km (120 MPa overburden pressure). The requirement, though, for deep explosion is that a triggering agent is necessary such as a strong earthquake or failure of the vent overburden (e. g. Mount St. Helens on 18 May 1980).

Assuming the validity of the magma-water interaction models outlined above, a two-stage explosion sequence may be the best explanation for hydrovolcanic explosions where an obvious trigger is lacking. The two stages are: (1) strong superheating (spontaneous nucleation vaporization) initiates at the top of the magma column where am-

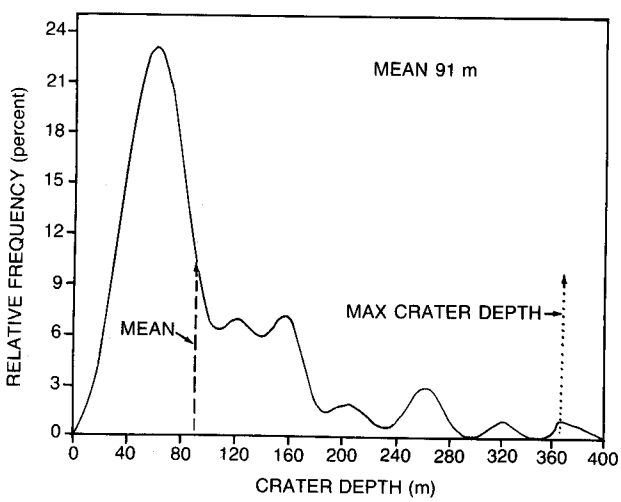

Fig. 7. Relative frequency diagram of maar crater depths from data compiled by Pike and Clow (1981). The mean of the positively skewed data set is about 91 m

bient pressure is less than the suppression limit (a still largely theoretical value); (2) downward propagation of strong pressure waves from stage 1 promotes thermal detonation of the magma-water mixture at depth.

There is good evidence from oxygen isotope analyses of erupted materials (Lipman and Friedman 1975; Hildreth et al. 1984) that intermixing of meteoric water can occur at deep levels in the magma conduit system. The hypothesis that vaporization at the limit of superheating might develop pressure waves of sufficient amplitude to trigger detonation is supported by the work of Shepherd and Sturtevant (1982). Their evaluation of the Landau instability, based on experimental and theoretical results, shows that the maximum far-field pressure developed by evaporative flux caused by the instability is given by: $p_{max}=dp/dt\ (t')$, where dp/dt was measured at 1.4×10^2 MPa/s, and t' was measured to be equal to $10^2r'$ (t' in μs and r' is the pre-expanded vapor film thickness in millimeters). A *C-J* state pressure of 10^2 MPa then requires a layer of water at the superheat limit of about 10 m thickness, which fits within limits considered possible by Bennett (1974) for water-magma mixes during submarine hydrovolcanic explosions. Furthermore, the harmonic tremor often recorded during eruption might be explained by the development of fluid instabilities occurring during boiling heat transfer from the magma to ground water along the margins of an intrusion (analogous to seismic tremor reported by Kieffer 1984). Landau and Taylor instabilities are well known to occur during initial stages of film boiling (Berenson 1961). A further discussion of instabilities will not be given here, but if film boiling proceeds at maximum heat flux, seismic waves of an appropriate frequency (1 to 10 Hz; McNutt 1985) may explain some types of harmonic tremor and initial triggering of strong melt-water intermixing at depth.

Illustration of some analytical techniques for field study

Using the general model for explosive hydromagmatic eruptions described above, a field example is given to illustrate how geological data can be applied to support and develop the hypothesis for water-magma interaction for a particular volcano. This example entails stratigraphic description and sample analysis of a scoria cone near Lathrop Wells, Nevada. The cone, as described later, is interpreted to display a history of initial hydromagmatic activity,

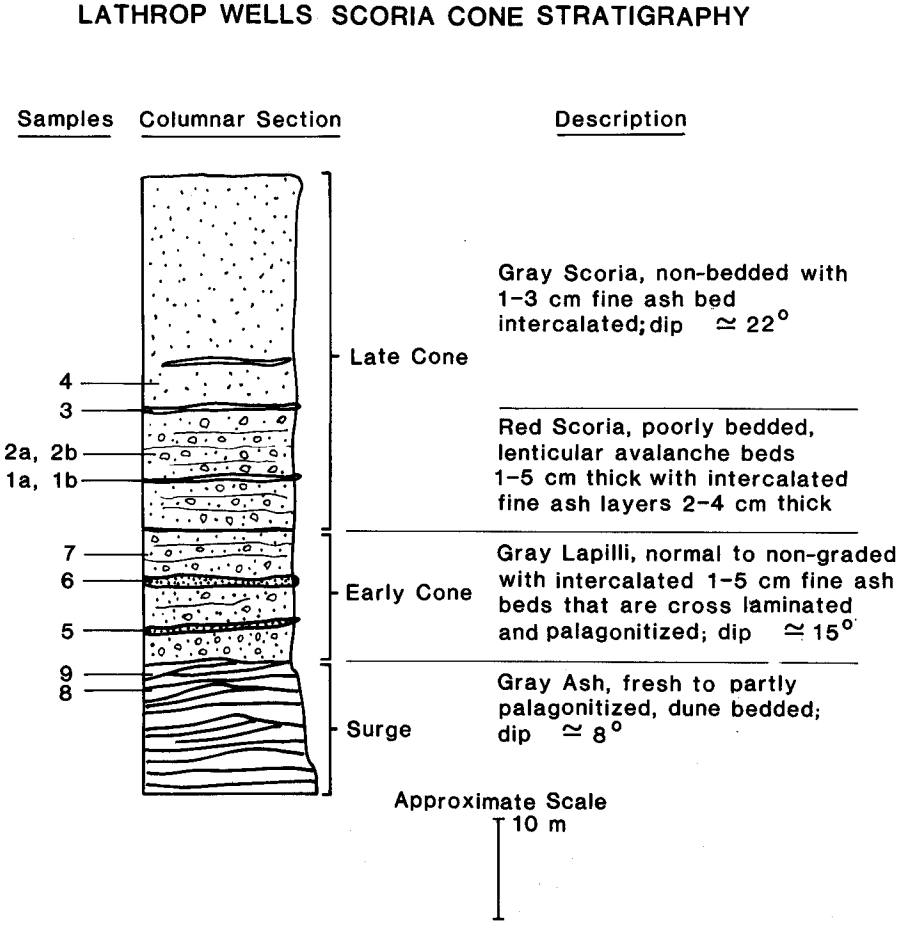

Fig. 8. Stratigraphic columnar section for the Lathrop Wells scoria cone shown schematically with an approximate scale

producing a tuff ring, followed by drier, Strombolian eruptions interspersed with sporadic pulses of fine-ash-producing, wet explosions. A similar case of Strombolian and intermittent phreatomagmatic activity has been extensively documented by Houghton and Hacket (1984).

Recently, methods of analyzing volcanic ash have incorporated particle size and component analyses as well as scanning electron microscopy (SEM) techniques (e. g. Walker and Croasdale 1971; Heiken 1972, 1974; Houghton and Hacket 1984). Wohletz (1983a, b) demonstrated the correlations of grain size distribution, shape, and surface chemistry data obtained by energy dispersive spectral (EDS) analysis with eruption energy and mechanism of particle formation.

Eleven tephra samples were obtained from the Lathrop Wells cone and represent early to late stage eruption products. The stratigraphic column with sampled intervals (Fig. 8) distinguishes three sample types corresponding to (1) finely bedded layers of pyroclastic surge bed form, (2) massive, poorly bedded to nonbedded scoria layers, and (3) fine ash layers intercalated with the scoria layers. Samples were sequentially subjected to size, petrographic, SEM, and EDS analysis as described below. Results are shown graphically and indicate intermittent hydrovolcanic explosions during the early phases of eruptive activity.

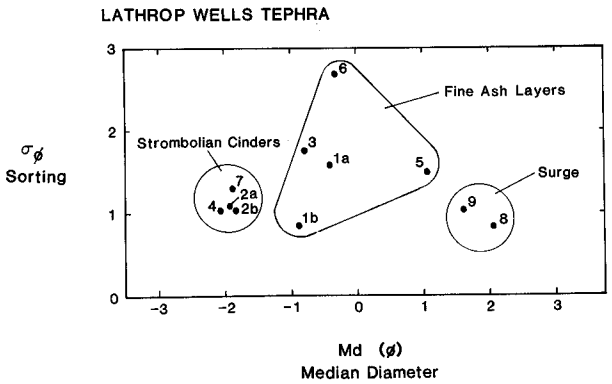

Fig. 9. Plot of Inman (1952) sorting coefficient versus median diameter showing the plotted fields of scoria, fine ash, and surge samples

Particle size

Samples were sieved at 1/2 ϕ [$\phi = -\log_2$ (diam. in mm)] intervals from $-3\ \phi$ (8 mm) to $4.5\ \phi$ (0.44 mm) with a standard Tyler sieve set. The contents of each sieve were weighed to 0.1 g accuracy and were saved for later petrographic analysis. Figure 9 is a plot of the Inman (1952) sorting coefficient (σ_ϕ) versus median diameter (Md_ϕ). Three fields are outlined in Fig. 9, showing the range of parameters for the three sample types mentioned above. "Surge" samples are the finest grained and best sorted; scoria samples are uniformly coarse grained and moderately sorted; and fine ash layers show a wide variation in median diameter and sorting, intermediate in values compared to those of the other two sample types.

Figure 10 is a plot of Md_ϕ and wt. % ash finer than 1.0 mm versus the stratigraphic sequence of samples. In this plot and subsequent ones of this type, values are weighted by the thickness of the sampled interval. Hence samples from thin stratigraphic intervals have values plotted as spikes, showing sharp discontinuities in the overall character.

Constituent analysis

The basaltic tephra at Lathrop Wells consists of basaltic glass, crystal fragments, and lithic clasts from underlying

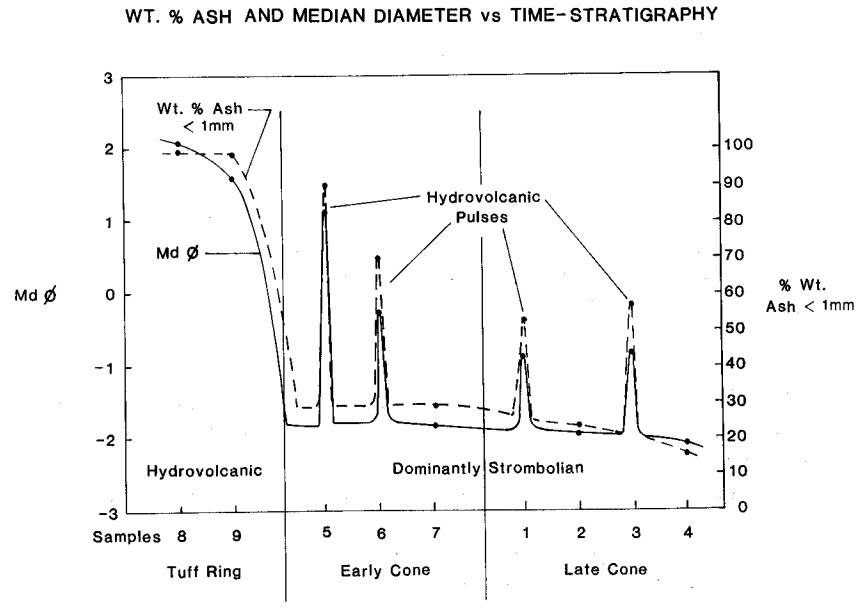

Fig. 10. Plot of median diameter and wt. % ash (<1.0 mm) versus stratigraphic sequence. Note that in this figure and Figs. 11–13, *spikes* in plotted *curves* show the inferred deviation from Strombolian "background" values. The *spikes* in the *curves* correspond to hydrovolcanic pulses

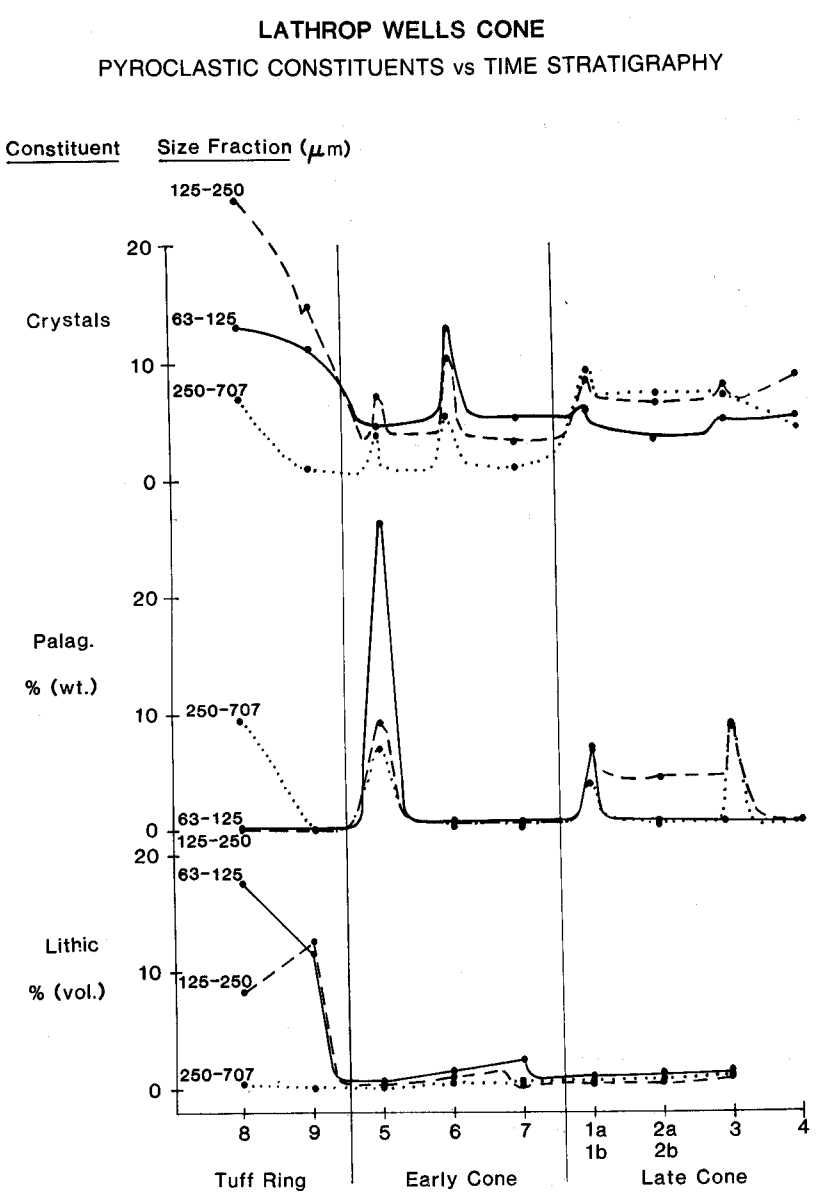

Fig. 11. Plot of tephra constituent abundances for three size fractions versus stratigraphic sequence. *Palag.* = palagonitic altered glass

rock units. The abundance of each of these constituents varies among samples and among the various size fractions within individual samples. The constituent abundances were obtained by grain counts using a binocular microscope. Three size fractions were counted: 63–125, 125–250, and 250–707 μm. Because of the large number of grains included in the field of microscopic view, accuracy is about ±0.1 vol. % for lithic materials. Figure 11 is a plot of constituent abundance with stratigraphy. This plot shows the variation of abundances for each of the three size fractions and the marked difference of "surge" and fine ash samples compared to the scoria samples.

Lithic constituents represent pieces of country rock broken and incorporated in the rising magma. This mixing occurs because of large hydraulic pressure gradients in wall rocks surrounding the rising magma body. For hydrovolcanic eruptions where ground water moves into and contacts rising magma, thermal-hydraulic fracturing of the wall rock and magma occurs (Delaney 1982). Thus, the lithic type and abundance indicate the stratigraphic level of hydrovolcanic interaction. Funiciello et al. (1976) have demonstrated that increased lithic abundances are characteristic of hydrovolcanic tephra. For the Lathrop Wells tephra, tuffaceous fragments from the Tiva Canyon Member of the Paintbrush Tuff dominate lithic constituents. Hence, ground water interaction with magma occurred dominantly in this stratigraphic interval, which is estimated to be at a depth of 20–50 m.

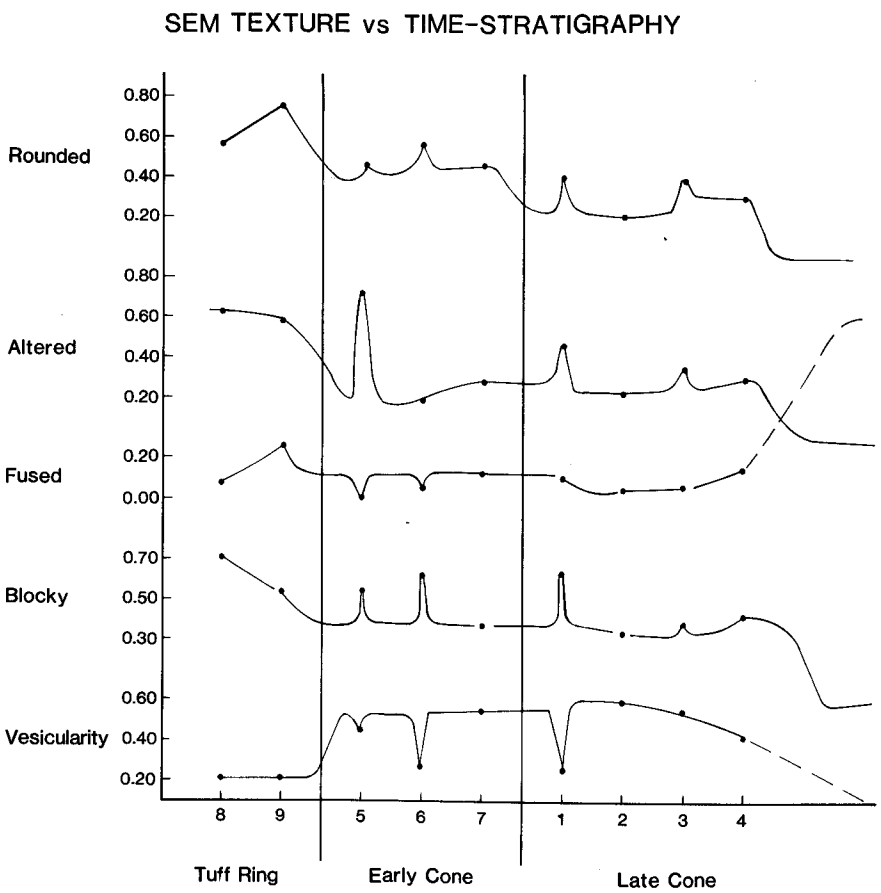

Fig. 12. Plot of tephra textural abundances versus stratigraphic sequence

Tephra surface textures

Following the method of Sheridan and Marshal (1983), samples were prepared for SEM inspection. Samples were split into a coarser fraction for low resolution microscopy and a fine fraction (<63 μm) for high resolution imaging using the upper stage of the SEM. The upper stage permitted adequate imaging to magnifications of about 100 kX which is necessary for particles in the size range of 0.1 to 1.0 μm. The technique for quantification of textural features is discussed by Wohletz (1983b).

Five textural features were chosen for quantification (presence or absence): vesicularity, angular blocky grain boundaries, fused surfaces, surface chemical alteration, and grain abrasion shown by overall rounding of initially sharp edges. Data for these five textural features, obtained by inspection of at least 50 representative grains for each sample, are shown in Fig. 12. Heiken (1972, 1974) noted that the blocky texture is a distinguishing characteristic of ash grains formed in hydrovolcanic eruptions. Vesicularity is a measure of volatile concentration in magma prior to eruption and completeness of magmatic volatile exsolution at low pressures before solidification. Fused surfaces form on ash particles when fragmentation occurs before melt surface temperature has fallen below the solidification temperature. Alteration is the chemical response of ash particle surfaces to hot volatiles and fluids during eruption and to ground water after tephra emplacement. At Lathrop Wells, most alteration must have occurred during and shortly after eruption because alteration zones are independent of a ground water table or vent location, and they correspond to fine ash layers that were probably emplaced from wet, steam-rich surges.

Surface chemistry

As part of the SEM analysis, EDS analysis of grain surfaces was done to give a semi-quantitative measure of grain surface alteration. The justification for quantitative analysis on particle surfaces using the peak to background method is described by Rez and Konopka (1984). They found that the peak to background ratio does not vary much with sample orientation; however, care was taken in this study to achieve uniform sample orientation to allow correlation among grains analyzed.

For each sample at least seven analyses were made and the results averaged. Using the standard deviation of element abundances from the EDS technique, an accuracy between ± 0.1 to 2.3 wt.% was obtained depending upon the element analyzed. Figure 13 is a plot of elemental

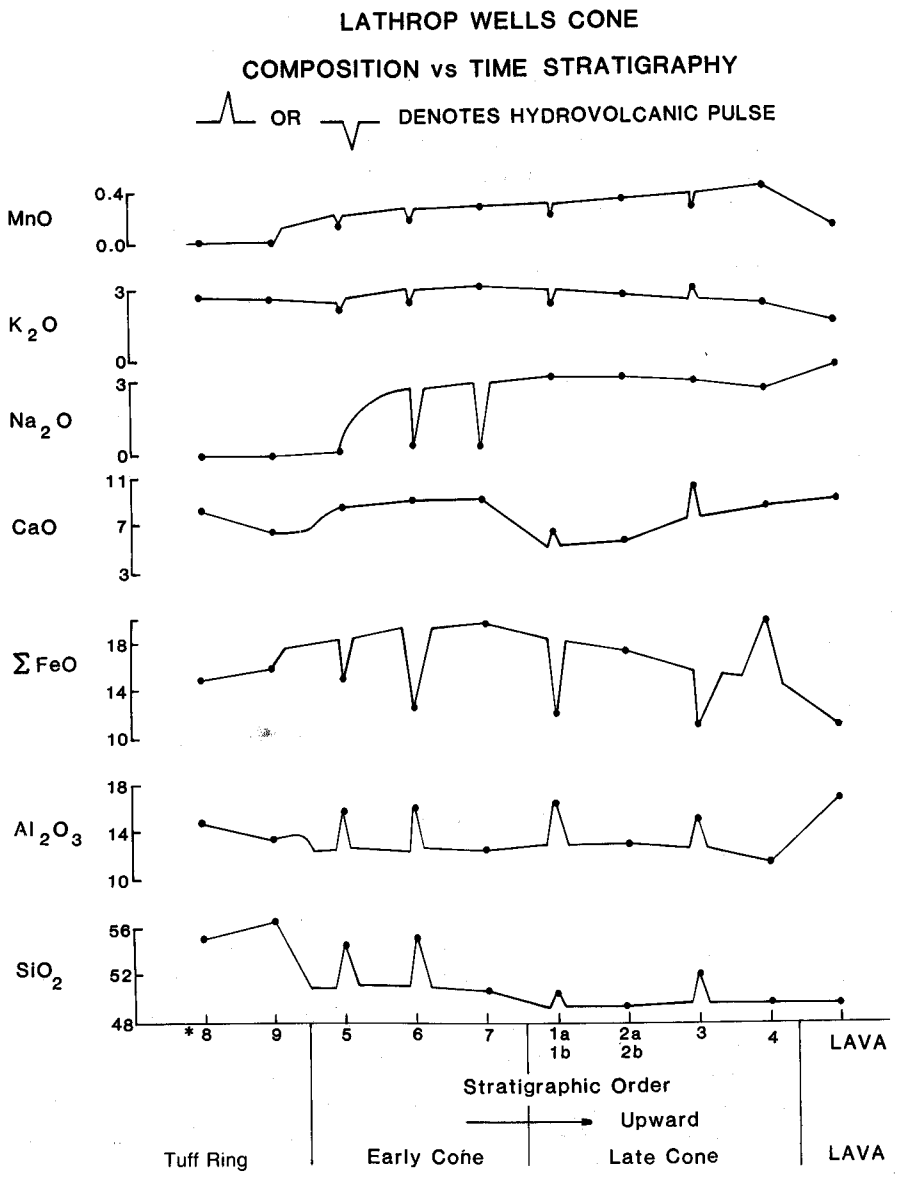

Fig. 13. Plot of tephra surface chemical abundances versus stratigraphic sequence

abundances versus stratigraphic position. This figure shows the variation of surface alteration among samples. Again, marked deviations in composition are noted for surge and fine ash samples compared to scoria samples, which show the least alteration from the fresh lava chemistry.

Discussion and intepretations of field data

The tephra data presented in this section form the basis for the detailed interpretation of eruption mechanism of the Lathrop Wells basalt center. Plots showing tephra data plotted as a function of stratigraphy (Figs. 10–13) all show: (1) a major discontinuity of plotted values at the transition from the earlier formed tuff ring to the cone building episodes; (2) sharp spikes in plotted values for fine ash samples compared to scoria samples; and (3) near uniformity of plotted values for samples of the same bed form. This is clear evidence that at least two fragmentation mechanisms produced the tephra.

The fact that scoria samples all showed relatively high vesicularity, minor alteration, few blocky breakage surfaces, and greater than 2 mm particle sizes is best explained by a magmatic eruption mechanism in which rising magma is torn apart by expanding gas as it approaches the surface. Although there are no unequivocal data supporting the origin of the gas, the fact that the tephra show no quenching effects, no alteration caused by disequilibrium between the liquid phase (glass) and vapor, and no brittle fracture textures makes it likely that the vapors were originally dissolved in the melt. Basalt melts may contain from one to several weight percent H_2O in solution, which exsolves

with decreasing pressure. This origin does not preclude a deep (>1–10 km) external source of water that may have passively diffused into the melt from country rock (Taylor 1971).

Pyroclastic surge and fine ash samples show distinctly different textures and surface chemical compositions from scoria samples. Blocky particle surfaces, surface chemical alterations, fine grain size (>1 mm), and low vesicularity indicate that these tephra were not formed by exsolving volatile components, but by a process that mechanically fractured the magma while quenching it and produced surface chemical changes by disequilibrium conditions. This type of tephra formation is best explained by a hydrovolcanic mechanism.

Apparently, opening eruptions at Lathrop Wells were hydrovolcanic. These produced uniformly fine grained (<250 μm; Fig. 10) ash that was dispersed in pyroclastic surges. Concurrent with surge deposition, much of the fine ash was probably convected into the atmosphere and carried by winds to far-field localities. Since grain size decreases with increasing violence of vapor explosions, because of the control of melt surface area on heat transfer rate, a thermodynamic efficiency of 1%–5% for these explosions at Lathrop Wells is indicated from data shown by Wohletz (1983b). Using curves shown in Fig. 6 and the correlation of the deposits with dry Strombolian activity, a water-melt mass ratio (R^*) of less than 0.2 can be estimated. Note that for curves shown in Fig. 6, this value of R^* is close to the explosive-nonexplosive transition (assuming detonation parameters discussed earlier). Furthermore, curves shown in Fig. 2 indicate that the Lathrop Wells situation might best be fit to the isothermal case, which can be expected for steam carried along with the surges, and that surges would be emplaced with mostly dry (superheated) steam. Accordingly, 1%–5% of the total thermal energy of the erupted basalt was converted to kinetic energy of the explosion. Basalt has a heat content of about 1×10^6 J/kg (1×10^{13} erg/kg) at magma temperatures near 1300 K. The surge deposit volume is about 0.01 km^3 and its bulk density is 1.5×10^3 kg/m^3 (Vaniman and Crowe 1981). Not accounting for loss of fine ash to distal parts, the eruption released about 1 to 5×10^{14} J of energy, roughly analogous to the energy released from about 35 to 175 ktonnes of high explosives. This amount of explosive energy can be correlated to crater dimensions by the empirical relationships derived for explosive excavation (Johnson 1971). Because hydrovolcanic explosions result in large vapor expansions, they should scale like high explosives do in low-strength alluvium. Based on this assumption, a crater diameter of nearly 350 m and a crater depth of about 70 m can be inferred from the deposit characteristics. The preceding calculations are supported by the fact that the present-day cone (diameter ≅ 500 m) covers the topographic rim of the tuff ring. Similarly, the inferred crater depth is near the depth of origin for lithic fragments found in the tephra. If the u_{el} requirement for explosive interaction (Fig. 6) is relaxed to about 40 m/s, then predicted median grain sizes of about 200 μm would also correlate to observed values. Hence, results of field and laboratory analysis of tephra can be related to energy and mechanism of eruption.

Following the opening explosive activity, the Lathrop Wells vent entered a less explosive, scoria cone building phase (Strombolian). The fine ash layers intercalated in the scoria beds represent short-lived vapor explosions that infrequently punctuated the dominantly Strombolian behavior. These hydroexplosions resulted from periods of ground water mixing into the vent's feeder system, which probably occurred during periods of slow magma rise when the magma's hydrostatic head decreased sufficiently to allow the water intrusion. The last activity at the cone was entirely nonexplosive effusion of lava, reflecting depletion of magma volatiles and effective sealing of the vent system from ground water incursions.

Conclusions

Hydrovolcanic eruptions produce distinctive tephra deposits that provide quantitative data such as grain-size distributions, grain shapes and surface chemistry, tephra constituent abundances, deposit thickness and aereal extent, bed-form types, sizes, and distribution, and depositional angles (cohesivity). These data can be interpreted with respect to the fluxes of magma and water within the volcano, the depth of interaction, and the geometry of the vent. The thermodynamics of hydrovolcanic systems, although very complex, show for simplistic analyses the systematic effect of varying mass ratios of water and magma. For mass ratios less than about 0.3 to 0.4, depending upon magma composition, expansion of steam can be expected to be in the dominantly superheated state, whereas for greater ratios expansion will produce saturated steam. Near this transition towards expansion in the two-phase field of water, the maximum amount of heat energy is converted into mechanical energy for the work of magma fragmentation, crater excavation, ejecta dispersal, and other dynamic processes. Although thermodynamic considerations need to be adapted to geologic situations, such as degree of magma-water mixing, depth of interaction, and mode of contact, the theory helps in placing constraints upon eruption phenomena deduced from field studies. Such deduction is a valuable aid for hazard evaluation and exploration for geothermal energy.

The analogy of hydrovolcanic activity to FCIs appears to be a useful approach to understanding eruption dynamics. Specifically, the liquid instability and thermal detonation analyses satisfactorily explain how magma and water can sufficiently intermingle to produce large explosions. There are many limitations to both analyses, especially when superheating is invoked; however, for the general

aspects of tephra grain morphologies and surface textures, the hydrodynamic theories are experimentally sound and provide an attractive basis by which to evaluate SEM data. The FCI analogy need not be limited to explosive phenomena. Nonexplosive mixing and heat transfer situations are important to granulation and brecciation in and around intrusions, extrusion of lava on the sea floor, migration of magmatic and wallrock chemical species, and water saturation of magmas in chambers and dikes within the earth's crust. Volcanologists are faced with documenting new evidence that supports the hypothesis of FCI behavior in volcanoes. Furthermore, they must be aware of the complexity of physical and chemical phenomena that can result from magma-water interaction. Finally, development of a general hydromagmatic theory can be applied to an understanding of many geothermal systems and ore deposits.

Acknowledgments. Michael Corradini of the University of Wisconsin, Richard Anderson of Argonne National Laboratory, Marshall Berman of the Sandia National Laboratories, and others of the Nuclear Regulatory Commission Working Group on Fuel–Coolant Interactions provided sound advice and encouragement for analogue studies. Robert McQueen, Marty Horn, and Bruce Crowe of Los Alamos National Laboratory, G. Froehlich of the University of Stuttgart, and Bradford Sturtevant of the California Institute of Technology also made helpful suggestions and offered interesting insights. Bruce Houghton and Peter Kokelaar provided stimulating discussions and helpful reviews of this manuscript. This work was supported by the U.S. Department of Energy through Institutional Supporting Research and Development at Los Alamos National Laboratory.

References

Bankoff SG, Jo JH (1976) Existence of steady-state fuel-coolant thermal detonation waves. ERDA Rep NU-2512-6 (CONF-760328-8), Nat Tech Inform Ser Springfield, Virginia

Bellman R, Pennington RH (1954) Effects of surface tension and viscosity on Taylor instability. Quart Appl Math 12: 151–162

Bennett FD (1974) On volcanic ash formation. Am J Sci 274: 648–661

Berenson PJ (1961) Film boiling heat transfer from a horizontal surface. J Heat Transfer: 351–358

Berman M (1983) Light water reactor safety research program semiannual report, April — September 1982. Sandia Nat Labs SAND83-1576 NUREG/CR-3407, Nat Tech Inform Ser Springfield, Virginia

Berman M (1984) Light water reactor safety research program semiannual report, October 1982 — March 1983. Sandia Nat Labs SAND84-0688 NUREG/CR-3734, Nat Tech Inform Ser Springfield, Virginia

Board SJ, Hall RW, Hall RS (1975) Detonation of fuel coolant explosions. Nature 254: 319-321

Boivin P, Bourdier JL, Camus A, de Goer de Herve A, Gourgaud A, Kieffer G, Mergoil J, Vincent PM, Auby R (1982) Influence de la nature des magmas sur activité phreatomagmatique: approche volcanologique et thermodynamique. Bull Volcanol 45: 25–40

Burnham CW (1983) Deep submarine pyroclastic eruptions. Econ Geol Mono 5: 142–148

Burnham CW, Holloway JR, Davis NF (1969) Thermodynamic properties of water to 1000 °C and 10 000 bars. Geol Soc Am Sp Pap 132: 1–96

Buxton LD, Benedict WB (1979) Steam explosion efficiency studies. Sandia Nat Labs SAND79-1399 NUREG/CR-0947, Nat Tech Inform Ser Springfield, Virginia, pp 1–62

Carlisle D (1963) Pillow breccias and their aquagene tuffs, Quadra Island, British Columbia. Am J Sci 71: 48–71

Chandrasekhar S (1968) Hydrodynamic and hydromagnetic stability, 2nd edn. Oxford University Press, Oxford, pp 1–652

Condiff DW (1982) Contributions concerning quasi-steady propagation of thermal detonations through dispersions of hot liquid fuel in cooler volatile liquid coolants. Int J Heat Mass Transfer 25: 87–98

Corradini ML (1978) Heat transfer and fluid flow aspects of fuel-coolant interactions. PhD Thesis, Massachusetts Inst Tech, Cambridge Mass, USA

Corradini ML (1981a) Phenomenological modelling of the triggering phase of small-scale steam explosion experiments. Nucl Sci Eng 78: 154–170

Corradini ML (1981b) Analysis and modelling of steam explosion experiments. Sandia Nat Labs SAND80-2131 NUREG/CR-2072, Nat Tech Inform Ser Springfield, Virginia, pp 1–114

Courant R, Friedrichs KO (1948) Supersonic flow and shock waves. Springer, New York, pp 1–464

Cronenberg AW (1980) Recent developments in the understanding of energetic molten fuel-coolant interactions. Nucl Saf 21: 319–337

Crowe BM, Wohletz KH, Vaniman, DT, Gladney E (1985) Status of volcanic hazard studies for the Nevada nuclear waste storage investigations: part II--FY85. Los Alamos Nat Lab Rep LA-9325-MSII, Nat Tech Inform Ser Springfield, Virginia, pp 1–67

Delaney PT (1982) Rapid intrusion of magma into wet rock: ground water flow due to pore pressure increases. J Geophys Res 87: 7739–7756

De Rita D, Funiciello R, Rossi U, Sposato A (1983) Structure and evolution of the Sacrofano-Baccano caldera, Sabatini volcanic complex, Rome. J Volcanol Geotherm Res 17: 219–236

Drumheller DS (1979) The initiation of melt fragmentation in fuel-coolant interactions. Nucl Sci Eng 72: 347–356

Fauske HK (1973) On the mechanism of uranium dioxide-sodium explosive interactions. Nucl Sci Eng 51: 95–101

Fauske HK (1977) Some comments on shock-induced fragmentation and detonating thermal explosions. Am Nucl Soc Trans 27: 666–667

Fisher JC (1948) The fracture of liquids. J Appl Phys 19: 1062–1067

Fowles GR (1979) Vapor phase explosions: elementary detonations? Science 204: 168–169

Frazzetta G, La Volpe L, Sheridan M (1983) Evolution of the Fossa cone, Vulcano. J Volcanol Geotherm Res 17: 329–360

Frenkel J (1946) Kinetic theory of liquids. Clarendon, Oxford

Froehlich G, Mueller G, Unger H (1976) Experiments with water and hot melts of lead. J Non-Equil Thermodyn 1: 91–103

Froehlich G, Mueller G, Unger H (1978) Analysis of shapes of solidified melts from entrapment experiments. Am Nucl Soc Trans 28: 449

Funiciello R, Locardi E, Lombardi G, Parotto M (1976) The sedimentary ejecta from phreatomagmatic activity and their use for location of potential geothermal areas. In: Proceedings Geothermal Energy, International Congress on Thermal Waters, Geothermal Energy and Vulcanism of the Mediterranean Area, Athens, pp 227–240

Heiken GH (1971) Tuff rings: examples from the Fort Rock-Christmas Lake Valley basin, south-central Oregon. J Geophys Res 76: 5615–5626

Heiken GH (1972) Morphology and petrography of volcanic ashes. Geol Soc Am Bull 83: 1961–1988

Heiken GH (1974) An atlas of volcanic ash. Smithson Contrib Earth Sci 12: 1–101

Henry RE, Miyazaki K (1978) Effects of system pressure on the bubble growth from highly superheated water droplets. In: SG Bankoff (ed) Topics in two-phase heat transfer and flow, Am Soc Mech Eng New York, pp 1–10

Hicks EP, Menzies DC (1965) Theoretical studies on the fast reactor maximum accident. In: Proceedings of the Conference on Safety, Fuels,

and Core Design in Large Fast Power Reactors, October 11–14, 1965, USAEC Rep ANL-7120, Nat Tech Inform Ser Springfield, Virginia, pp 654–670

Hildreth W, Christiansen RL, O'Neil JR (1984) Catastrophic isotopic modification of rhyolitic magma at times of caldera subsidence, Yellowstone Plateau volcanic field. J Geophys Res 89: 8339-8370

Holloway JR (1977) Fugacity and activity of molecular species in supercritical fluids. In: Fraser DG (ed) Thermodynamics in geology, Reidel Dordrecht-Holland, pp 161–181

Houghton BF, Hacket WR (1984) Strombolian and phreatomagmatic deposits of Ohakune craters, Ruapehu, New Zealand: a complex interaction between external water and rising basaltic magma. J Volcanol Geotherm Res 21: 207–231

Inman DL (1952) Measures for describing the size distribution of sediments. J Sediment Petrol 22: 125–145

Johnson SM (1971) Explosive excavation technology. US Army Eng Nucl Crat Group Rep 21, Nat Tech Inform Ser Springfield, Virginia, pp 229

Kieffer SW (1984) Seismicity at Old Faithful geyser: an isolated source of geothermal noise and possible analogue of volcanic seismicity. J Volcanol Geotherm Res 22: 59–95

Kieffer SW, Delany JM (1979) Isentropic decompression of fluids from crustal and mantle pressures. J Geophys Res 84: 1611–1620

Knapp RB, Knight JE (1977) Differential thermal expansion of pore fluids: fracture and microearthquake production in hot pluton environments. J Geophys Res 82: 2515–2522

Kokelaar BP (1982) Fluidization of wet sediments during the emplacement and cooling of various igneous bodies. J Geol Soc London 139: 21–33

Kokelaar BP (1983) The mechanism of Surtseyan volcanism. J Geol Soc London 140: 933–944

Ladisch R (1977) Comment on fragmentation of UO by thermal stress and pressurization. Nucl Eng Des 43: 327–328

Landau LD, Lifshitz BM (1959) Fluid mechanics: vol 6, Course of theoretical physics. Pergamon, New York

Lipman PW, Friedman I (1975) Interaction of meteoric water with magma: an oxygen isotope study of ash-flow sheets from southern Nevada. Geol Soc Am Bull 86: 695–702

McNutt S (1985) Volcanic tremor: basic facts and perspective. EOS Trans Am Geophys Union 66(46): 1152

Moore JG, Nakamura K, Alcaraz A (1966) The 1965 eruption of Taal Volcano. Science 151: 955–960

Nelson LS, Duda PM (1981) Steam explosion experiments with single drops of CO_2 laser-melted iron oxide. Am Nucl Soc Trans 38: 453-454

Oh M-D (1985) Thermal-hydraulic modelling and analysis for large-scale vapor explosions. Univ Wisconsin Reac Saf Res Thesis 29: 1–395

Patel PD, Theofanous TG (1978) Fragmentation requirements for detonating thermal explosions. Nature 274: 142–144

Pike RJ, Clow GD (1981) Revised classification of terrestrial volcanoes and catalog of topographic dimensions, with new results on edifice volume. US Geol Surv Open File Rep 81-1038: 1–40

Rabie RL, Fowles GR, Fickett W (1979) The polymorphic detonation. Phys Fluids 22: 422–435

Reid RC (1976) Superheated liquids. Am Sci 64: 146–156

Rez P, Konopka J (1984) Limitations in the use of the peak-to-background method for quantitative analysis. X-ray Spect 13: 33–37

Self S (1983) Large-scale phreatomagmatic silicic volcanism: a case study from New Zealand. J Volcanol Geotherm Res 17: 433–469

Self S, Wilson L, Nairn IA (1979) Vulcanian eruption mechanisms. Nature 277: 440–443

Self S, Kienle J, Huot JP (1980) Ukinrek maars, Alaska, II. deposits and formation of the 1977 craters. J Volcanol Geotherm Res 7: 39–65

Sharon A, Bankoff SG (1981) On the existence of steady supercritical plane thermal detonations. Int J Mass Heat 24: 1561–1572

Shepherd JE, Sturtevant B (1982) Rapid evaporation at the superheat limit. J Fluid Mech 121: 379–402

Sheridan MF, Barberi F, Rosi M, Santacroce R (1981) A model for Plinian eruptions of Vesuvius. Nature 22: 282–285

Sheridan MF, Marshall JR (1983) SEM examination of pyroclastic materials: basic considerations. In: Scanning Electron Microscopy 1983. SEM, Chicago, pp 113–118

Sheridan MF, Wohletz KH (1981) Hydrovolcanic explosions: the systematics of water-pyroclast equilibration. Science 212: 1387-1389

Sheridan MF, Wohletz KH (1983) Hydrovolcanism: basic considerations and review. J Volcanol Geotherm Res 17: 1–29

Sourirajan S, Kennedy GC (1962) The system H_2O-NaCl at elevated temperatures and pressures. Am J Sci 260: 115–141

Sturtevant B, Frost D (1984) Effects of ambient pressure on the instability of a liquid boiling explosively at the superheat limit. In: Proceedings of the Symposium on Fundamentals of Phase Change: Boiling and Condensation, Am Soc Mech Eng Winter Annual Meeting 1984

Taylor HP (1971) Oxygen isotope evidence for large-scale interaction between meteoric ground waters and Tertiary granodiorite intrusions, western Cascade range, Oregon. J Geophys Res 76: 7855–7874

Thorarinsson S, Einarsson T, Sigvaldason G, Elisson G (1964) The submarine eruption off the Vestmann Islands 1963–64. A preliminary report. Bull Volcanol 27: 437–446

Vaniman D, Crowe BM (1981) Geology and petrology of the basalts of crater flat: applications to volcanic risk assessment for the Nevada nuclear waste storage investigations. Los Alamos Natl Lab Rep LA-8845-MS, Nat Tech Inform Ser Springfield, Virginia, pp 1–267

Verbeek RDM (1885) Krakatau. Batavia, pp 1–495

Walker GPL, Croasdale R (1971) Characteristics of some basaltic pyroclastics. Bull Volcanol 35: 305–317

Waters AC, Fisher RV (1971) Base surges and their deposits: Capelinhos and Taal Volcanoes. J Geophys Res 76: 5596–5614

Williams H, McBirney AR (1979) Volcanology. Freeman, San Francisco, pp 1–391

Wohletz KH (1983a) Mechanisms of hydrovolcanic pyroclast formation: grain-size, scanning electron microscopy, and experimental results. J Volcanol Geotherm Res 17: 31–63

Wohletz KH (1983b) Chemical and textural surface features of pyroclasts from hydromagmatic eruption sequences. In: Marshall JR (ed) Characterization and quantification of surface features on Clastic and Pyroclastic particles. Hutchinson, San Francisco and Los Alamos Nat Lab LA-UR 83-250, Los Alamos, New Mexico

Wohletz KH, McQueen RG (1984) Experimental studies of hydromagmatic volcanism. In: Explosive volcanism: inception, evolution, and hazards. Studies in Geophysics. National Academy Press, Washington, pp 158–169

Womer MB, Greeley R, King JS (1980) The geology of Split Butte – a maar of the south-central Snake River plain, Idaho. Bull Volcanol 43: 453-472

Received February 9, 1986/Accepted July 1, 1986